





Maximum-entropy-based metrics for quantifying critical dynamics in spiking neuron dataFelipe Serafim ¹, Tawan T. A. Carvalho ^{1,2,3}, Mauro Copelli ¹ and Pedro V. Carelli ^{1,*}¹*Departamento de Física, Centro de Ciência Exatas e da Natureza, Universidade Federal de Pernambuco, Recife PE 50670-901, Brazil*²*Life and Health Sciences Research Institute (ICVS), School of Medicine, University of Minho, 4710-057 Braga, Portugal*³*ICVS/3B's-PT Government Associate Laboratory, 4806-909 Braga/Guimares, Portugal*

(Received 1 April 2024; accepted 8 July 2024; published 1 August 2024)

An important working hypothesis to investigate brain activity is whether it operates in a critical regime. Recently, maximum-entropy phenomenological models have emerged as an alternative way of identifying critical behavior in neuronal data sets. In the present paper, we investigate the signatures of criticality from a firing rate-based maximum-entropy approach on data sets generated by computational models, and we compare them to experimental results. We found that the maximum entropy approach consistently identifies critical behavior around the phase transition in models and rules out criticality in models without phase transition. The maximum-entropy-model results are compatible with results for cortical data from urethane-anesthetized rats data, providing further support for criticality in the brain.

DOI: [10.1103/PhysRevE.110.024401](https://doi.org/10.1103/PhysRevE.110.024401)**I. INTRODUCTION**

The brain is a complex system that operates through the interactions of nonlinear systems at various scales, from neurons to circuits and brain areas. It coordinates to generate behavior, thought, and cognition. An important working hypothesis regarding the nervous system's organization is that brain dynamics operate at or near a phase transition, specifically at a critical point.

This hypothesis has gained traction, particularly with the pioneering work of Beggs and Plenz [1], who measured power-law distributions in the neuronal avalanches of local field potential data from cultured cortical slices. They found power-law exponents compatible with a critical branching process. The notion that the brain operates within an organizational regime characterized at the edge between order and disorder carries potential benefits, including computational advantages such as enhanced transmission capacity [2], a larger repertoire of functional states [3,4], and a maximized dynamic range [5–7].

Given this scenario, numerous experiments have been conducted to evaluate exponents for both size and duration distributions, testing the critical brain hypothesis. In experiments conducted on the awake mouse and rat cortex [8,9], the avalanche exponents were consistent with those obtained by Beggs and Plenz. However, there are divergent findings regarding the avalanche exponents in rats anesthetized with different drugs [8–10]. Furthermore, significantly different avalanche exponents were observed in *ex vivo* recordings from the turtle visual cortex, as well as in M/EEG data analysis in resting or behaving humans [11,12]. More recently, the crackling noise scaling relation between critical exponents has been

incorporated as a more rigorous way of identifying criticality in neuronal avalanche data [13].

However, neuronal avalanches have methodological limitations, particularly when applied to spiking activity. One limitation is the lack of timescale separation, as there is no real silence in the brain. Another, and perhaps the most studied, is subsampling, which means that we are only measuring a subset of the network activity [10,14–17]. Additionally, according to [18], in subsampled data, it is possible to obtain apparent exponents compatible with those found by Beggs and Plenz for the Brunel model [19] in its synchronous irregular phase, which occurs far away from the phase transition.

More recently, phenomenological maximum entropy models have been utilized to describe the statistics of neuronal data sets. These models offer an alternative approach to assess signatures of criticality, utilizing the divergence of a generalized specific-heat measure. The maximum entropy method provides a probabilistic model that reproduces a set of observable statistics of the analyzed data while remaining maximally unstructured [20]. This approach avoids biases for unstated assumptions. Different maximum entropy models have been developed based on the observed variables of interest and have been used in various neural network systems [21–25]. Once we obtain the maximum entropy model to describe the data set, we can calculate a generalized specific heat, and a divergence of this measure with the size of the system is used as a signature of criticality [21,26,27]. However, the sensitivity of the maximum entropy results to the distance to criticality in neuronal data sets has not been systematically studied.

In this work, we assess the accuracy of the maximum-entropy model developed by Mora *et al.* [26], which is based on the global activity of the network, considering temporal dynamics, in neural models whose phase transitions we know analytically (including whether or not they have one, to start with). In the initial stage, we verified the method's capability to reveal a critical point. Through this investigation,

*Contact author: pedro.carelli@ufpe.br

we obtained parameters that allow us to identify criticality in subsampled data, in conditions similar to the experimental data sets. Subsequently, we assessed the ability of the maximum-entropy method to rule out criticality even when the data exhibited power laws. Finally, we applied the analysis to spiking data from urethane-anesthetized rats, categorizing them as operating in the critical regime based on the obtained references.

II. METHODS

A. A spiking neuronal network with excitation and inhibition

Here we will briefly describe the neuronal model presented by Girardi-Schappo *et al.* [28]. This model consists of N neurons undergoing stochastic integrate-and-fire dynamics with a discrete time equal to 1 ms. Neurons are divided into excitatory ($N_E = 0.8N$) and inhibitory ($N_I = 0.2N$) subpopulations and are connected in an all-to-all graph. The neuron states are defined by the boolean variable $X(t) = 1$ for those that are spiking at time t , and $X(t) = 0$ for those that are not. The membrane potential for neuron i in the excitatory (E) and inhibitory (I) population is given by

$$V_i^{E/I}(t+1) = \left[\mu V_i^{E/I}(t) + I_e + \frac{J}{N} \sum_{j=1}^{N_E} X_j^E(t) - \frac{gJ}{N} \sum_{j=1}^{N_I} X_j^I(t) \right] (1 - X_i^{E/I}(t)), \quad (1)$$

where J represents the synaptic coupling strength, g is the inhibition-to-excitation (I/E) coupling strength ratio, μ denotes the leak time constant, and I_e stands for an external current.

The differential aspect of this model, compared to other integrate-and-fire models, lies in the existence of a probability of the neuron firing given its potential V . This probability is governed by the function

$$\Phi(V) \equiv P(X = 1|V) = \Gamma(V - \theta)\Theta(V - \theta)\Theta(V_S - V) + \Theta(V - V_S), \quad (2)$$

where $\theta = 1$ represents the firing threshold, Γ is the firing gain constant, $V_S = 1/\Gamma + \theta$ denotes the saturation potential, and $\Theta(x > 0) = 1$ (zero otherwise) is the Heaviside step function. To initiate activity in the network, a seed is sent to just one single excitatory neuron through the external current $I_e > V_S$, which after starting activity is maintained at $I_e = \theta$. This procedure is repeated whenever network activity dies off. For simplicity, we consider $\mu = 0$, which does not change the phase transition of the model.

This model leads to an active phase where excitation dominates (characterized by a low value of g), and an absorbing phase where inhibition dominates (characterized by a high value of g). The transition between these phases occurs at $g_c = 1.5$ (for $\Gamma = 0.2$ and $J = 10$) at a directed percolation critical point, as demonstrated previously [28].

We selected this model because it has a well-defined critical point, thereby providing a theoretical reference for the results obtained from the maximum entropy analysis.

Additionally, it accurately reproduces experimental activity and avalanche results [17] in the data that will be analyzed here. We simulated this model with a time of $t = 10000$ s, equivalent to the time of the experimental data analyzed later. Here, the network has $N = 10^5$, and we used the following parameter values: $\Gamma = 0.2$, $J = 10$, $\Theta = 1$, and $I_e = 1$.

B. Probabilistic cellular automaton model

In this subsection, we will describe the neuronal model introduced by Kinouchi and Copelli [5]. Similar to the model presented in the previous subsection, this model belongs to the same mean-field direct percolation (MF-DP) universality class and operates with discrete time steps ($\Delta t = 1$ ms). Our objective with this model is to assess the robustness of the results obtained from the maximum-entropy analysis for the model described in the previous section.

The network consists of N probabilistic excitable cellular automata, each of which randomly connects with K presynaptic sites. Each site possesses n possible states divided into three different regimes: the resting state ($s_i = 0$), the excited state ($s_i = 1$), and $n - 2$ refractory states ($s_i = 2, 3, \dots, n-1$). The excitation of a site can occur in two ways: via an external stimulus, modeled by a Poisson process with rate r [$p_h(r) = 1 - \exp(-r\Delta t)$], or via stimuli from its presynaptic neighbors, with p_{ij} representing the probability of this stimulus if neighbor j is active at time t . The other transitions occur with probability 1.

The control parameter is determined by the branching parameter $\sigma = K\langle p_{ij} \rangle$, where p_{ij} is a random variable with uniform distribution in the interval $[0, 2\sigma/K]$. The mean-field analysis indicates that the model belongs to the MF-DP universality class. In this analysis, $\sigma = 1$ is the critical point of the system, $\sigma < 1$ corresponding to the subcritical regime, where the system inevitably reaches the absorbing state (all sites quiescent), and for $\sigma > 1$ we have the active state (the activity continues propagating in the network) that characterizes the supercritical phase.

Here, we simulate with $N = 10^5$ sites, $K = 10$ presynaptic neighbors, $n = 5$ possible states, and $r = 0$ (no external stimuli). Whenever the network reaches the absorbing state, a site is randomly activated ($s_i = 1$) in order to start a new activity.

C. Brunel model

We also apply the maximum-entropy analyses to the non-critical model proposed by Brunel [19]. This model consists of excitatory and inhibitory neurons governed by the leaky integrate-and-fire dynamics

$$\tau_m \frac{dV_i(t)}{dt} = -V_i(t) + \tau \sum_j J_{ij} \sum_k \delta(t - t_j^k - D), \quad (3)$$

where τ_m represents the membrane time constant, and D corresponds to the transmission delay. The membrane potential of neuron i is denoted as V_i . When V_i reaches the threshold θ , a spike is generated, and the membrane potential is reset to V_r . During the refractory period τ_r the cell is insensitive to stimulation. The second term in Eq. (3) accounts for the connection with the other neurons in the network. The δ function computes the time of arrival of the k th spike of neuron j , t_j^k ,

at the neuron i at time t . The synaptic coupling strength from neuron j to neuron i is given by J_{ij} . For excitatory synapses, we have $J_{iE} = J$, and for inhibitory synapses, $J_{iI} = -gJ$. The parameter g acts as a control parameter in the model, regulating the balance between excitatory and inhibitory components in the network.

The network consists of $N = 12\,500$ neurons, where $N_E = 0.8N$ are excitatory neurons and $N_I = 0.2N$ are inhibitory neurons. The connections between the neurons in the network are sparse and random. Each neuron receives internal connections from $C_E = 0.1N_E$ excitatory neurons and $C_I = 0.1N_I$ inhibitory neurons. Also, each neuron receives $C_{\text{ext}} = C_E$ connections from excitatory neurons outside the network. The external synapses are activated by an independent Poisson process with rate ν_{ext} .

The external rate ν_{ext} will be compared with the rate needed for a neuron to reach the threshold in the absence of feedback, which is $\nu_{\text{thr}} = \theta/(JC_E\tau)$. The ratio $\nu_{\text{ext}}/\nu_{\text{thr}}$ serves as a secondary control parameter. The interplay between these two control parameters leads to distinct dynamical patterns within the network and among individual neurons. In terms of network behavior, the firing activity can be either synchronous or asynchronous. On the other hand, when considering individual cells, one can observe varying degrees of regularity or irregularity in their spike patterns.

We selected this model for our analyses based on the discovery of power-law avalanche distributions in the synchronous irregular phase, i.e., in a noncritical region (outside a phase transition) [18]. This finding highlights the importance of recognizing that power-law avalanches alone do not necessarily indicate criticality. As we will demonstrate, the Brunel model does not exhibit criticality when subjected to the maximum-entropy analysis. This serves to illustrate that such an analysis has the capability to identify and dismiss criticality.

D. Data acquisition

The data used here are the same as those utilized in Ref. [17]. As has been described previously [17], we used six Long-Evans (*Rattus norvegicus*) rats (male, 280–360 g, 24 months old). The animals were anesthetized with urethane (1.55 g/kg), diluted at 20% in saline, in three intraperitoneal (i.p.) injections, 15 min apart [29]. Some animals demanded supplement (max 5%) urethane to reach the proper level of analgesia. The primary visual cortex (V1) was marked by coordinates: AP = -7.2 , ML = 3.5 relative to Bregma [30]. We performed recordings of extracellular voltage of neuronal populations by using a 64-channel multielectrode silicon probe (Neuronex technologies, Buzsaki64spL-A64). This probe has 60 electrodes disposed in six shanks separated by 200 μm , 10 electrodes per shank with an impedance of 1–3 $\text{M}\Omega$ at 1 kHz. Each electrode has 160 μm^2 and they are in staggered positions 20 μm apart. We recorded from deeper layers of the rat cortex, similarly to what was previously done in Ribeiro *et al.* [10] under ketamine-xylazine and Fontenele *et al.* [13] under a setup similar to the one presented here.

Data were sampled at 30 kHz, and amplified and digitized in a single head-stage (Intan RHD2164) [31]. We recorded spontaneous activity during long periods (≥ 3 h). We used

the open-source software KLUSTA to perform the automatic spike sorting on raw electrophysiological data [32]. The automatic part is divided into two major steps: spike detection and automatic clustering. Manual spike sorting allows the identification of each cluster of neuronal activity as single-unit activity (SUA) or multi-unit activity (MUA). We used both SUA and MUA clusters for our study.

E. Spiking-time maximum entropy model

The maximum-entropy method provides a bias-free probability distribution that reproduces a set of observed data statistics. In neuroscience, these statistics are typically extracted from the binary spike matrix $\{s_{i,t}\}$. The time series is segmented into temporal windows Δt . If neuron i spiked at least once within window t , then $s_{i,t} = 1$ (otherwise, $s_{i,t} = 0$).

Here we use a maximum-entropy model that is based on the firing rate of the network in different time steps. To capture the temporal dynamics, the maximum-entropy model by Mora *et al.* [26] uses observables like the joint distribution of the number of spiking neurons ($K_t = \sum_{i=1}^N s_{i,t}$) at different times windows, denoted as

$$P_u(K, K') = \frac{1}{L-u} \sum_{t=1}^{L-u} \sum_{\{s_{i,t}\}} \delta_{K,K_t} \delta_{K',K_{t+u}} P(\{s_{i,t}\}), \quad (4)$$

where $u = 1, \dots, v$ controls the temporal distance between two windows, and L is the number of times bins.

The probability distribution to be inferred is written in Boltzmann form,

$$P_\beta(s_{i,t}) = \frac{1}{Z(\beta)} \exp[-\beta E(\{s_{i,t}\})], \quad (5)$$

where $Z(\beta)$ is the normalization constant. Here $\beta \equiv 1/T$ is an adjustable parameter equivalent to the inverse of temperature T . When $\beta = 1$, the model describes spike statistics. By varying β close to 1, different probability distribution models are obtained, enabling us to assess the proximity of the current state to the critical regime. To satisfy the observables, the “energy of spike trains” E is defined as follows:

$$E = - \sum_t^L h(K_t) - \sum_t^L \sum_{u=1}^v J_u(K_t, K_{t+u}), \quad (6)$$

where the terms $h(K_t)$ and $J_u(K_t, K_{t+u})$ are Lagrange multipliers associated with the constraints $P_u(K, K')$. With the appropriate Lagrange multipliers, $P_{u,\text{model}}$ is computed using the transfer-matrix technique (see [26,27] for details), while $P_{u,\text{data}}$ is directly calculated from the data.

Note that we are faced with an inverse problem. It is necessary to calculate the Lagrange multipliers such that $P_{u,\text{model}}$ is consistent with $P_{u,\text{data}}$. Model learning is achieved through an interactive process that is implemented based on the difference between the probabilities estimated by the model and the probabilities obtained from the data,

$$h(K_t) \leftarrow h(K_t) + \epsilon [P_{\text{data}}(K_t) - P_{\text{model}}(K_t)], \quad (7)$$

$$J_u(K_t, K_{t+u}) \leftarrow J_u(K_t, K_{t+u}) + \epsilon [P_{\text{data}}(K_t, K_{t+u}) - P_{\text{model}}(K_t, K_{t+u})]. \quad (8)$$

Such a procedure is equivalent to performing gradient descent on the log-likelihood [26]. Choosing a small enough value of ϵ ensures the convergence of $h(K_t)$ and $J_u(K_t, K_{t+u})$.

Once the probability distribution P_β is estimated, the specific heat can be calculated as a function of β ,

$$c(\beta) = \frac{\beta^2}{NL} \langle \delta E^2 \rangle_\beta, \quad (9)$$

where $\delta E \equiv E - \langle E \rangle_\beta$ represents the fluctuation from the mean energy, and its average is taken under P_β . For a system operating in the critical regime, it is expected that there will be a divergence of the specific heat as the network size increases, thus indicating the thermodynamic limit.

By varying T ($\beta \equiv 1/T$), we are exploring a family of probability distributions in search of the divergence of specific heat. The system is interpreted as critical as the peak of c approaches $T = 1$ with increasing N .

To investigate the dependence of c on the system size, samples of neurons were collected from simulations, chosen randomly. The creation of different subsamplings starts from the smallest subpopulation to be analyzed, adding neurons to form larger subpopulations. This ensures that the larger subpopulations include the same neurons as the smaller ones. For each model parameter, this process was repeated ten times. The consistency of our results is verified through the repetition of the same procedure for surrogate data, where for each neuron the sequence of interspike intervals was shuffled.

F. Critical metrics

We conduct the maximum entropy analysis by systematically exploring the control parameters in neural models. As will be shown in Sec. III, we obtained specific-heat curves that could lead to interpretations suggesting criticality in data that were previously known to be noncritical. For a systematic analysis, and to eliminate this ambiguity, we propose three metrics here that, when combined, are capable of characterizing the critical dynamics or lack thereof. In addition, they provide us with a quantitative analysis approach, which can be applied in the investigation of experimental data.

The first metric takes into consideration the relative distance between the critical temperature T^* and the temperature $T = 1$ that fits the data. Thus, we define

$$D_N = 1 - |1 - T_N^*|. \quad (10)$$

Note that in the ideal case, $|1 - T^*|$ will become zero, hence $D = 1$. The second metric takes into consideration that at the critical point, the $c(T)$ curves become sharper as N increases. To quantify this aspect, we calculate the width at half-height through $|T^* - T^\dagger|$ as illustrated in Fig. 1. Here, T^\dagger is defined by $c(T^\dagger) = c(T^*)/2$, corresponding to half of the maximum value of the $c(T)$ curve. Thus, we define the second metric as

$$W_N = 1 - |T_N^* - T_N^\dagger|. \quad (11)$$

Notice that as N grows, W tends to 1.

As we will see in the next section, these two factors alone are not enough to classify the analyzed data as operating in criticality. In the supercritical regime, curves with $T \approx 1$ were obtained, and we obtained very sharp curves with $T^* \approx 1$. To distinguish between critical and supercritical regimes, we

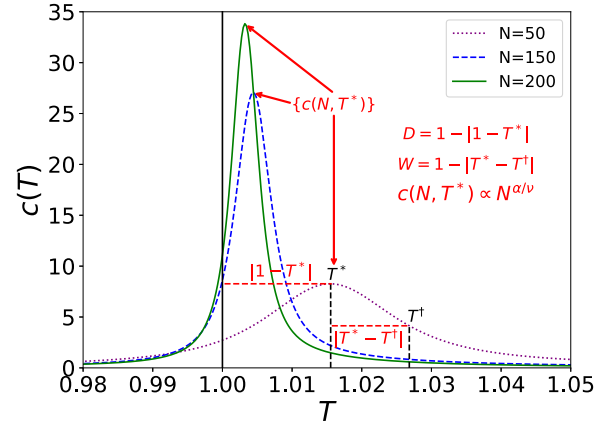


FIG. 1. Examples of specific-heat curves as a function of T and N . For the quantitative comparison of curves, we define three metrics. The metric D considers the distance from the specific-heat peak temperature T^* to $T = 1$, which fits the data. In the metric W , we consider the width of the curve at half-height by extracting $|T^* - T^\dagger|$, where T^\dagger is defined as the temperature at which $c(T^\dagger) = c(T^*)/2$. The last metric is based on the finite-size scaling theory, which takes into account that the specific-heat peak $c(N, T^*)$ for a population N of neurons scales with $N^{\alpha/\nu}$, where α and ν are critical exponents.

propose a third metric based on the monotonic increase of the specific-heat peak as N increases. According to the theory of finite-size scaling [33], at the critical point,

$$c(N, T^*) \propto N^{\alpha/\nu}, \quad (12)$$

where α and ν are critical exponents. On logarithmic scales, Eq. (12) is expected to yield a linear relationship between c and N at the critical point. To confirm the linear trend of the set of specific-heat peaks for each value of N , we applied Pearson's test [34]. The linear trend is provided with the value of r , which ranges from -1 to 1 , where $r = 1$ and -1 indicate perfect positive and negative correlations, respectively, and $r = 0$ indicates that there is no linear correlation between the variables. Therefore, we will utilize r as the third metric.

It is worth noting that each metric was defined to yield the value 1 as the ideal case for the specific aspect being captured. In Sec. III, we will see that these metrics can reach a value of 1 for noncritical regimes, but not simultaneously. Only in the critical regime do these three metrics achieve a value of 1. Therefore, for the critical regime, the product

$$DWr \rightarrow 1 \quad (13)$$

as N increases.

III. RESULTS

Maximum-entropy models have been used to identify criticality in experimental data sets [21,27,35]. However, a thorough investigation of direct comparisons with neuron models has been lacking. Here we evaluate the results from the maximum-entropy model described in Sec. II E in data sets from different neuron models. We evaluate the method's ability to identify signatures (or absence) of criticality in data

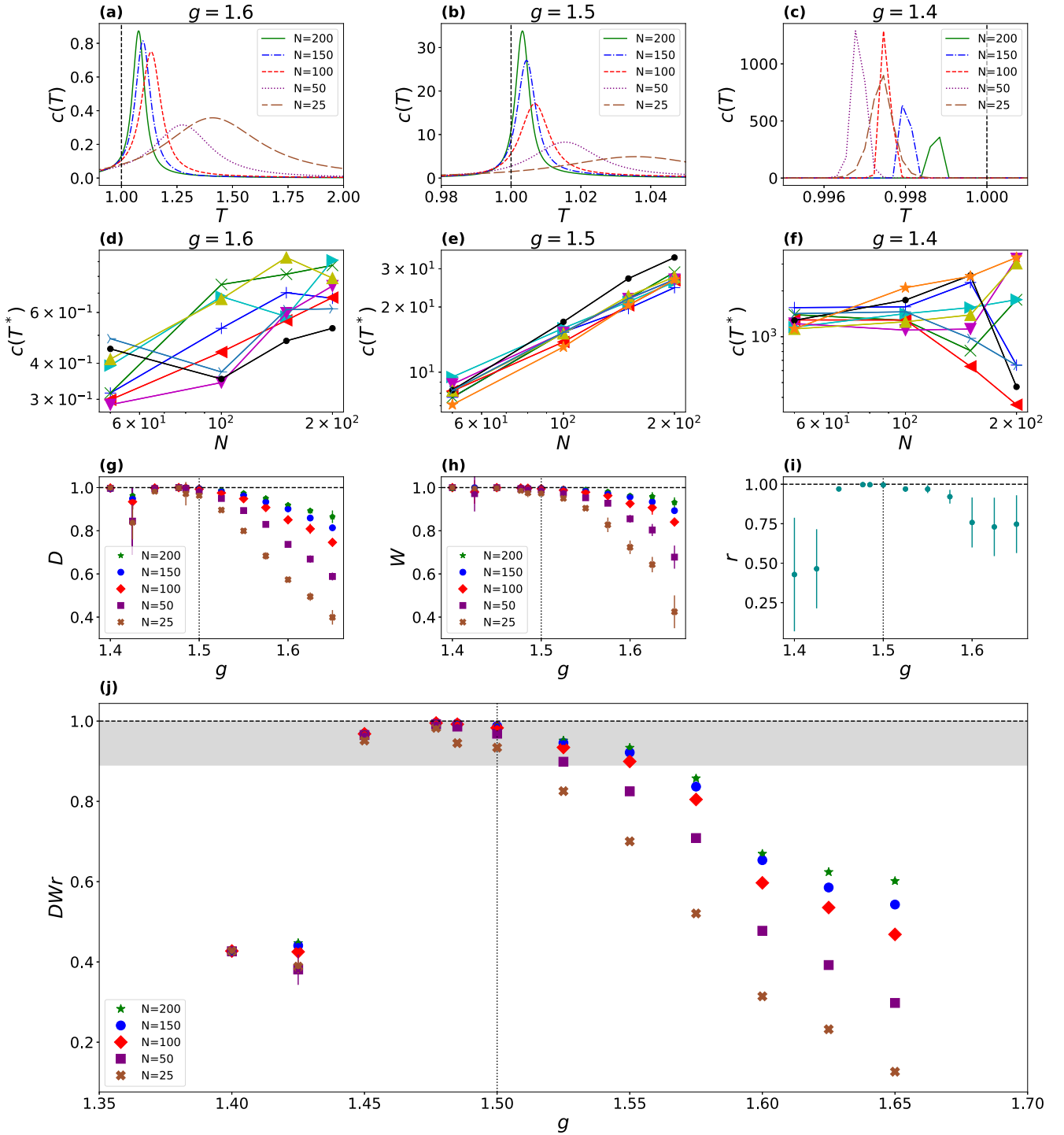


FIG. 2. Results for the spiking neuronal network (Sec. II A): Parts (a)–(c) illustrate specific-heat curves corresponding to the subcritical ($g = 1.6$), critical ($g = 1.5$), and supercritical ($g = 1.4$) regimes, respectively. Parts (d)–(f) depict $c(N, T^*) \times N$ on a logarithmic scale for different sample sets (symbols and colors correspond to the individual sets) obtained from the data across diverse dynamic regimes. The linear trend is exclusively noticeable for the critical regime (e), aligning with finite-size theory. Part (g) shows metric D assessing the proximity of T^* to $T = 1$, while (h) exhibits metric W representing width at half-height of the curves concerning g and N . Part (i) reveals metric r evaluating the linear trend in $c(N, T^*) \propto N^{\alpha/\nu}$, where α and ν are critical exponents. Finally, (j) illustrates the combination of the three metrics DWr . The dashed line in (g)–(j) indicates the model’s critical point. The gray band establishes the criterion observed in the models that indicate the critical regime.

from both critical and noncritical models, and we compare to experimental results.

Our analyses rely initially on the models presented in Secs. II A and II B, which are known to exhibit critical behavior. Near the critical point, these models exhibit dynamics that resemble the characteristics and diversities observed in experimental data, such as the statistics of avalanches [17].

Notably, at the critical point and its proximities, DWr shows considerable values (≈ 0.7) for smaller N values, a trend that diminishes as the control parameters move away from the critical point. In this study, we will subject them to maximum-entropy analyses to assess their agreement with criticality, as determined by avalanche statistics.

The maximum-entropy approach identifies a data set as operating in the critical regime with a progressive increase of the peak of $c(T^*)$ as N grows, with $T^* \approx 1$. This trend implies a divergence in the thermodynamic limit. Although this interpretation seems clear, we need to identify how the growth occurs and how close to $T^* \approx 1$ we must be in limited data sets to imply criticality.

Figures 2(a)–2(c) illustrate the specific-heat curves, respectively, for the subcritical ($g = 1.6$), critical ($g = 1.5$), and supercritical ($g = 1.4$) cases of the model described in Sec. II A. It is noticeable in both sub- and supercritical regimes that there is a growth of the specific-heat peak around $T = 1$, which could lead to a misinterpretation of criticality. However, it is possible to distinguish each of these cases. In Sec. II F, we introduced three metrics capable of making such a distinction.

Lotfi *et al.* proposed a measure aimed at calculating the normalized distance to criticality [27]; however, this measure was only applied to experimental data without a theoretical reference, and we verified the need to improve measures of criticality as shown here. The D and W metrics proposed here draw inspiration from elements of that measure. They are successful in characterizing the subcritical regime ($g \geq 1.60$), Figs. 2(g) and 2(h), since these factors differ from $D = 1$ and $W = 1$ (the critical result), tending to move away as the control parameter moves away from the critical point in the direction of the subcritical dynamics. However, they lack the sensitivity to distinguish the supercritical ($g < 1.40$) regime from the critical regime ($g = 1.5$), with D and W tending to 1 in either case.

In this context, we introduce the third metric, r . This metric is based on the linearity of the plot $c(N, T^*) \times N$ on a logarithmic scale, where we expect to observe a linear behavior for the critical point, as indicated by the theory of finite-size scaling. Figure 2(e) clearly demonstrates a linear trend for the critical points of the model across different sets of N . The same trend is not observed for the other dynamic regimes, as shown in Figs. 2(d) and 2(f).

Figure 2(i) displays r for the different dynamic regimes. We can observe that only this metric is capable of distinguishing between the different regimes. However, in the vicinity of the critical point, it is not as pronounced. For this reason, the product of the three metrics DWr provides a better distinction, as we can see in Fig. 2(j).

To check the consistency of these results, we applied the same methodology to the cellular automaton model described in Sec. II B, which also features a critical point ($\sigma = 1.00$) and

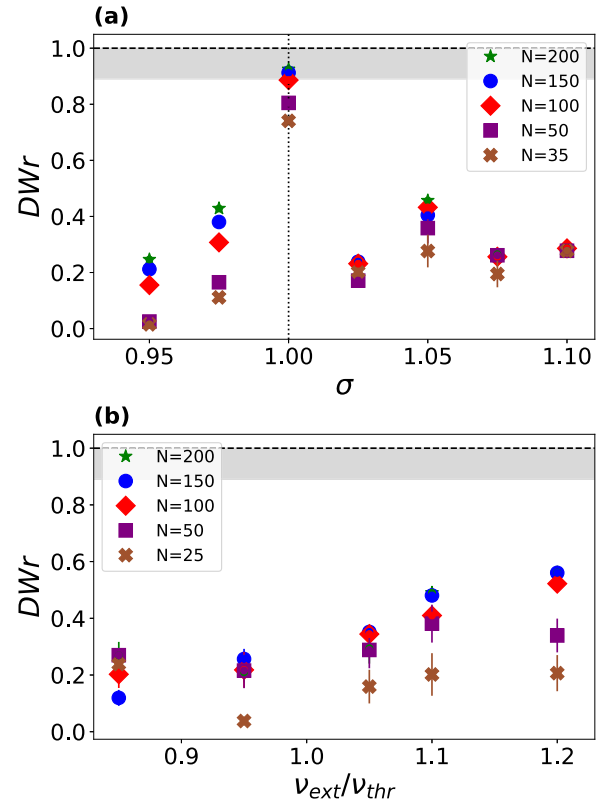


FIG. 3. Combination of the DWr metrics vs the control parameter of the cellular automaton and Brunel models. Part (a) presents the outcome for the cellular automaton model described in Sec. II B. The dashed line indicates the model's critical point. Here, we observe the method's consistency in distinguishing the critical point ($\sigma = 1.0$) from other dynamic regimes, evidenced by $DWr \simeq 1$. (b) Results for the Brunel model described in Sec. II C. In this case, DWr does not approximate 1, as expected, given the absence of a critical point in the model. These outcomes illustrate the method's consistency in detecting the critical or noncritical regime. The gray band establishes the criterion observed in the models that indicates the critical regime.

the same universality class as the previously analyzed model, albeit with a very different underlying topology. Figure 3(a) shows DWr for different dynamics regimes. As observed at the critical point ($\sigma = 1.00$), $DWr \rightarrow 1$, while the various noncritical regimes remain distant from this level (more details can be found in Fig. 5). This result demonstrates the methodology's efficiency in identifying critical dynamics.

We also subject it to Brunel's integrate-and-fire model described in Sec. II C. Such a model does not exhibit a critical point. In this model, Touboul and Destexhe [18] claim to find power-law distributions in its irregular synchronous phase with critical exponents consistent with the experimental data of Beggs and Plenz—a result that can be mistaken for criticality. We investigate the behavior of the specific heat exploring the synchronous irregular (SI) and asynchronous irregular (AI) phases as well as the border between them. We vary the control parameter ν_{ext}/ν_{th} within the interval $[0.85, 1.2]$, fixing $g = 6$, traversing from the SI to the AI phases [19]. Figure 3(b) displays the result for this model. It can be observed that for no control parameter (ν_{ext}/ν_{th}) does DWr tend towards 1, as expected. Hence, complemented by the three metrics

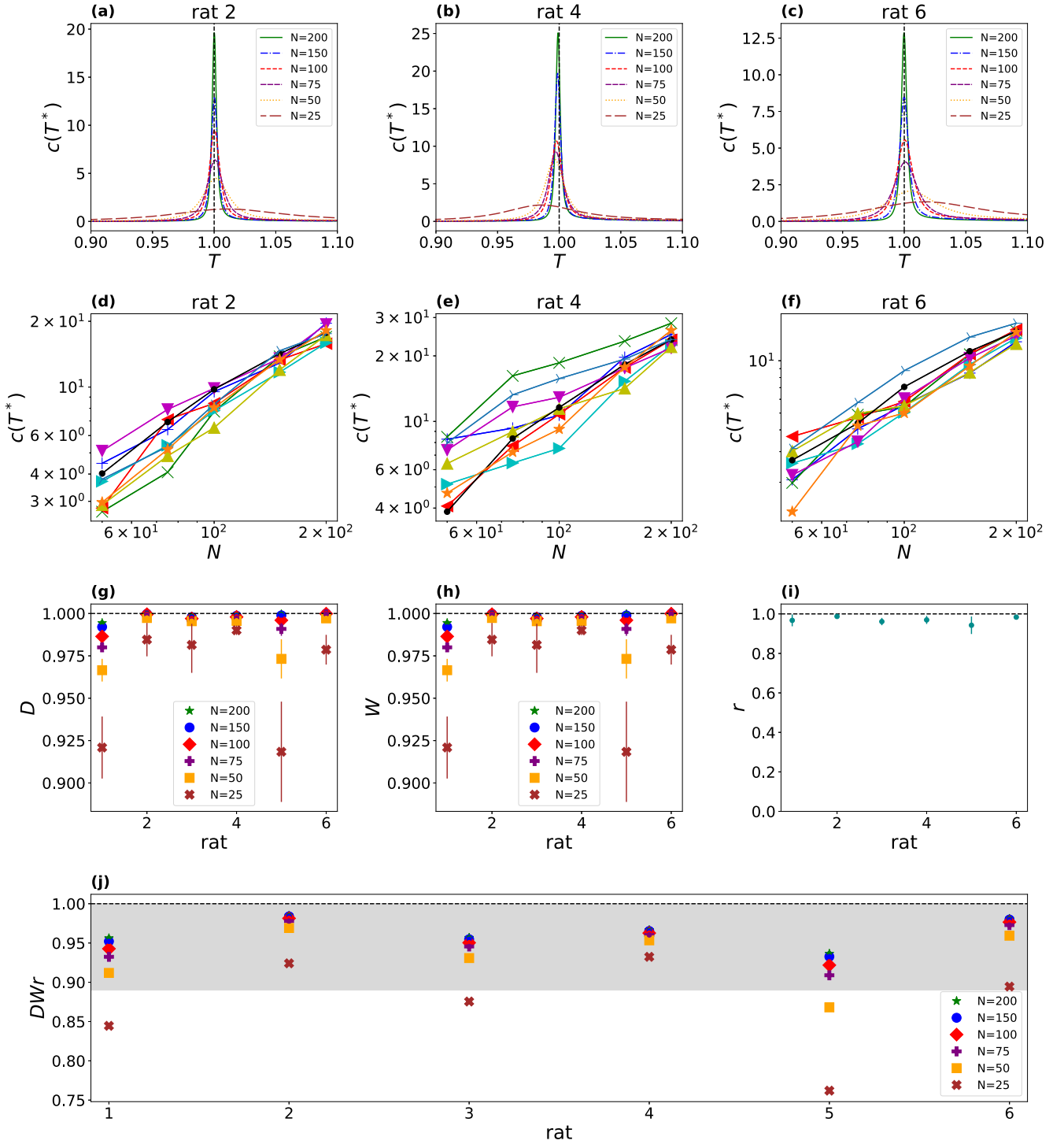


FIG. 4. Maximum-entropy results for V1 spiking data of urethane-anesthetized rats. (a)–(c) Specific-heat curves for different rats. (d)–(f) $c(N, T^*) \times N$ on a logarithmic scale for different rats. (g) Metric D assessing the proximity of T^* to $T = 1$, while (h) exhibits metric W representing width at half-height of the curves concerning different rats and N . (i) Metric r evaluating the linear trend in $c(N, T^*) \propto N^{\alpha/\nu}$. Finally, (j) illustrates the combination of the three metrics DWr . The gray band establishes the criterion observed in the models that indicate the critical regime.

introduced here, the maximum-entropy approach successfully ruled out criticality.

Based on observations from the neural models investigated here, it is viable to establish a quantitative criterion to classify experimental data as operating within the critical regime or its vicinity. In Fig. 2(j), we observe that DWr varies slowly as a

function of the control parameter; however, in Fig. 3(a), DWr changes abruptly. These results are related to the sensitivity of the models to the control parameter affecting their dynamics. A slower change of dynamics as a function of the control parameter allows us to investigate the sensitivity of DWr as we slowly move away from the critical point. In Fig. 2(j), we

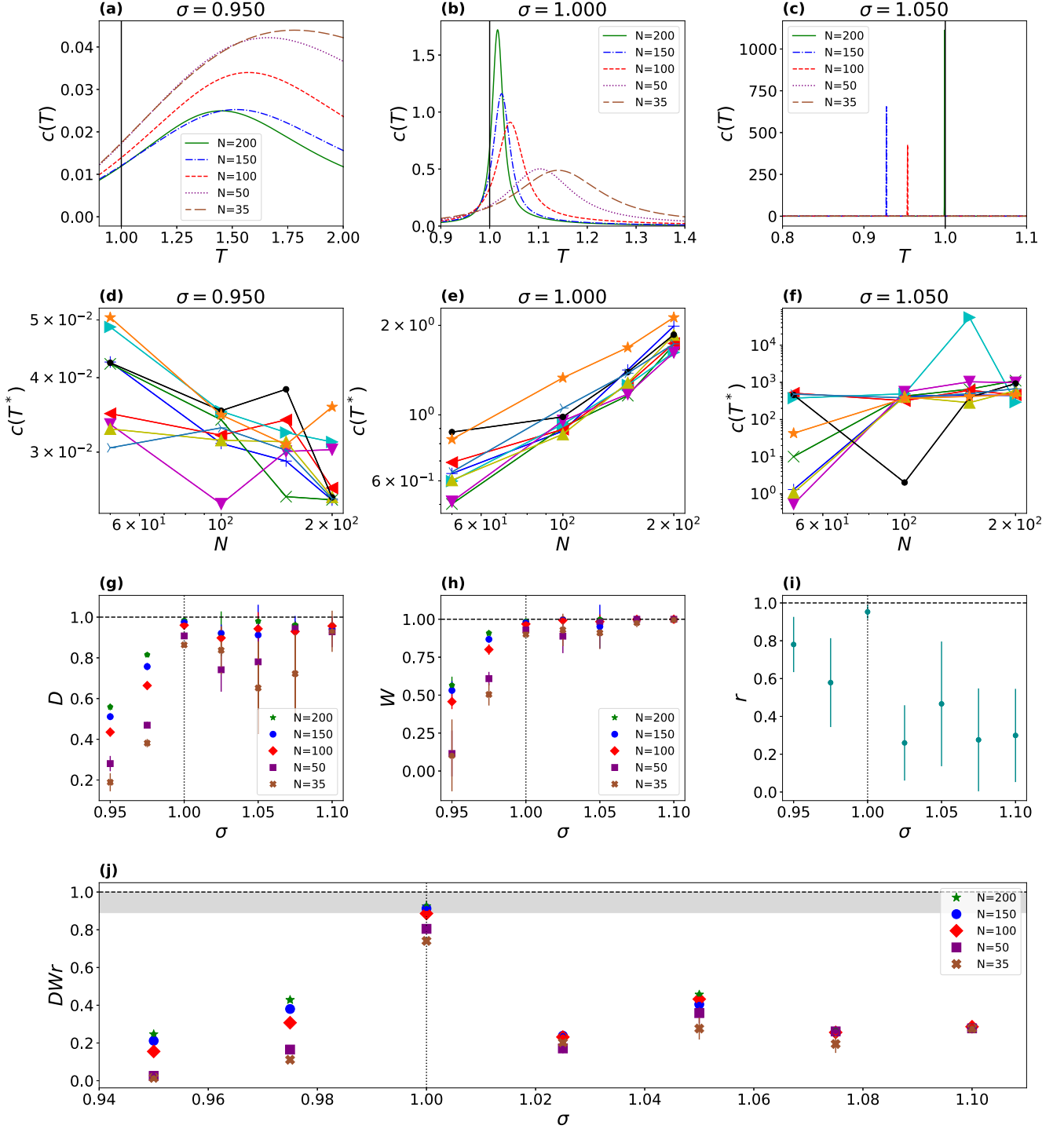


FIG. 5. Results for the cellular automaton model (Sec. II B). (a)–(c) Specific-heat curves corresponding to the subcritical ($\sigma = 0.950$), critical ($\sigma = 1.000$), and supercritical ($\sigma = 1.050$) regimes, respectively. (d)–(f) $c(N, T^*) \times N$ on a logarithmic scale for different sample sets obtained from the data across diverse dynamic regimes. The linear trend is exclusively noticeable for the critical regime (e), aligning with finite-size theory. (g) Metric D assessing the proximity of T^* to $T = 1$, while (h) metric W representing width at half-height of the curves concerning g and N . (i) Metric r evaluating the linear trend in $c(N, T^*) \propto N^{\alpha/\nu}$, where α and ν are critical exponents. Finally, (j) combination of the three metrics DWr . The gray band establishes the criterion observed in the models that indicate the critical regime. The dashed line in (g)–(j) indicates the model’s critical point.

notice that DWr begins to move away from 1 reaching values lower than 0.89 (gray band) as we vary the control parameter by 5% ($g = 1.425$ and 1.575) in relation to the critical point.

Furthermore, we notice that within this interval, DWr reaches values greater than 0.89 already with $N = 50$, which does not occur outside this interval even with $N = 200$. Therefore, to

classify experimental data operating within the critical regime or its neighborhood, we set a threshold of $DWr \geq 0.89$. This criterion raises the requirement to be considered critical, since it is possible to obtain relatively high values of DWr , as in the case of the shuffled data in Fig. 6(a), where we obtained $DWr \approx 0.8$.

Having established this criterion, we analyzed spiking data from the primary visual cortex (V1) of rats anesthetized with urethane (see Sec. IID). This drug induces various cortical states in the brain, ranging from high levels of spiking variability (synchronous state) to low levels of spiking variability (desynchronized state). Data similar to this have been utilized to establish the presence of criticality within an intermediate level of spiking variability for both avalanches [13] and maximum-entropy analyses [27]. In contrast to Ref. [27], which accessed different levels of spiking variability by segmenting the data based on the coefficient of variation, here we analyzed the entire time series.

Here, we used a standard of 200 neurons in each experimental data set. This number of neurons is of the same order of magnitude as the total number of neurons we obtained experimentally in all data sets, providing a consistent analysis, being computationally feasible for the maximum-entropy model, and already being a reliable size when compared to the analysis of computational model data. This aspect is significant as it allows us to establish criteria when the analysis is performed with a few neurons.

Figures 4(a)–4(c) depict the specific-heat curves for three out of the six analyzed rats. The metrics D and W [Figs. 4(g) and 4(h)] reach values very close to 1, similarly to what is observed in both the critical and supercritical regimes of the neural models [Figs. 2(g) and 2(h) and Figs. 5(g) and 5(h)]. The third metric, r , reaches values close to 1 [Fig. 4(i)]. This trend is confirmed in Figs. 4(d)–4(f).

By combining the metrics in Fig. 4(j) and adopting the quantitative criteria established (gray range), it can be inferred that all analyzed experiments are operating within the critical dynamics. Moreover, we observe that akin to the critical point in the models, such criteria are already met with smaller neuronal subsets. These results align with the analyses conducted on avalanches [13,17].

IV. CONCLUSION

Here, we investigated the ability of the maximum-entropy model developed by Mora *et al.* [26,27] in distinguishing critical and noncritical behavior, in particular using limited data sets. Using models that we analytically know to be critical, we developed and calibrated a criticality indicator DWr based on the analysis of generalized specific-heat curves. We were also able to rule out criticality in the Brunel model, which some authors argued could have misleading results with avalanches analysis over limited data sets [18]. Despite the proposed DWr metric demonstrating robustness in detecting criticality in known models, it alone does not distinguish between subcritical and supercritical states. However, as shown in Figs. 2 and 5, these cases can be detected by calculating the difference between the peak temperature and $T = 1$.

With the indicator DWr established and tested, we employed the same methodology on long recordings of cortical

spiking data from urethane-anesthetized rats. For all experimental data sets analyzed, we obtained $DWr \rightarrow 1$, indicating critical dynamics in the data. This result agrees with the conclusions drawn from different criticality signatures observed in similar data [13,27,36].

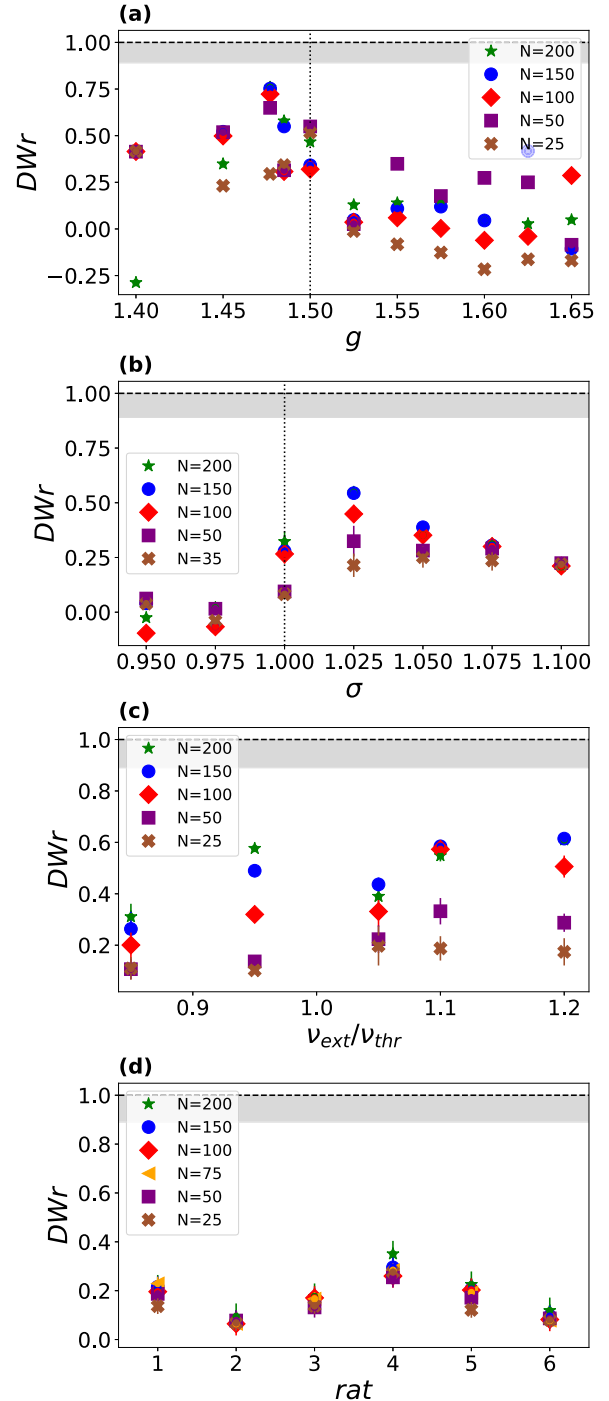


FIG. 6. DWr results for shuffled data vs the control parameter of the models (a)–(c) and experimental set (d). The dashed line in (a) and (b) indicates the model's critical point. The gray band establishes the criterion observed in the models that indicates the critical regime.

ACKNOWLEDGMENTS

The authors acknowledge support from Brazilian agencies CAPES (Grant No. PROEX 23038.003069/2022-87), CNPq (Grants No. 308703/2022-7, No. 249991/2013-6, No. 425037/2021-5, No. 311418/2020-1, No. 314094/2023-7, and No. 141579/2017-0), and FACEPE (Grants No. APQ-1187-1.05/22 and No. BFD-0013-1.05/20).

APPENDIX: APPLICATION OF MAXIMUM ENTROPY METHOD METRICS TO THE KC MODEL AND SHUFFLED DATA

Figure 5 shows the results in an extended form for the cellular automaton model described in Sec. II B.

Figures 5(a)–5(c) shows the specific-heat curves for three different dynamic regimes illustrating the variety of possible results. In Figs. 5(d)–5(f) we can observe the linear trend of specific-heat peaks $c(N, T^*)$ as a function of the analyzed subpopulation N . This result clearly demonstrates that this trend only occurs at the critical point. Figures 5(g) and 5(h) individually present the three metrics D , W , and r , respectively. Finally, Fig. 5(j) combines the three metrics, which clearly distinguishes the critical point from the other dynamic regimes.

Figure 6 shows the results of DWr for shuffled data from all three models, as well as from experiments. We note that in no case does $DWr \rightarrow 1$.

- [1] J. M. Beggs and D. Plenz, Neuronal avalanches in neocortical circuits, *J. Neurosci.* **23**, 11167 (2003).
- [2] W. L. Shew, H. Yang, S. Yu, R. Roy, and D. Plenz, Information capacity and transmission are maximized in balanced cortical networks with neuronal avalanches, *J. Neurosci.* **31**, 55 (2011).
- [3] W. L. Shew and D. Plenz, The functional benefits of criticality in the cortex, *Neuroscientist* **19**, 88 (2013).
- [4] C. Haldeman and J. M. Beggs, Critical branching captures activity in living neural networks and maximizes the number of metastable states, *Phys. Rev. Lett.* **94**, 058101 (2005).
- [5] O. Kinouchi and M. Copelli, Optimal dynamical range of excitable networks at criticality, *Nat. Phys.* **2**, 348 (2006).
- [6] W. L. Shew, H. Yang, T. Petermann, R. Roy, and D. Plenz, Neuronal avalanches imply maximum dynamic range in cortical networks at criticality, *J. Neurosci.* **29**, 15595 (2009).
- [7] D. B. Larremore, W. L. Shew, and J. G. Restrepo, Predicting criticality and dynamic range in complex networks: effects of topology, *Phys. Rev. Lett.* **106**, 058101 (2011).
- [8] G. Scott, E. D. Fagerholm, H. Mutoh, R. Leech, D. J. Sharp, W. L. Shew, and T. Knöpfel, Voltage imaging of waking mouse cortex reveals emergence of critical neuronal dynamics, *J. Neurosci.* **34**, 16611 (2014).
- [9] T. Bellay, A. Klaus, S. Seshadri, and D. Plenz, Irregular spiking of pyramidal neurons organizes as scale-invariant neuronal avalanches in the awake state, *eLife* **4**, e07224 (2015).
- [10] T. L. Ribeiro, M. Copelli, F. Caixeta, H. Belchior, D. R. Chialvo, M. A. Nicolelis, and S. Ribeiro, Spike avalanches exhibit universal dynamics across the sleep-wake cycle, *PLoS ONE* **5**, e14129 (2010).
- [11] J. M. Palva, A. Zhigalov, J. Hirvonen, O. Korhonen, K. Linkenkaer-Hansen, and S. Palva, Neuronal long-range temporal correlations and avalanche dynamics are correlated with behavioral scaling laws, *Proc. Natl. Acad. Sci. USA* **110**, 3585 (2013).
- [12] A. Zhigalov, G. Arnulfo, L. Nobili, S. Palva, and J. M. Palva, Relationship of fast-and slow-timescale neuronal dynamics in human MEG and SEEG, *J. Neurosci.* **35**, 5385 (2015).
- [13] A. J. Fontenele, N. A. P. de Vasconcelos, T. Feliciano, L. A. A. Aguiar, C. Soares-Cunha, B. Coimbra, L. Dalla Porta, S. Ribeiro, A. J. Rodrigues, N. Sousa, P. V. Carelli, and M. Copelli, Criticality between cortical states, *Phys. Rev. Lett.* **122**, 208101 (2019).
- [14] V. Priesemann, M. H. Munk, and M. Wibral, Subsampling effects in neuronal avalanche distributions recorded in vivo, *BMC Neurosci.* **10**, 40 (2009).
- [15] A. Levina and V. Priesemann, Subsampling scaling, *Nat. Commun.* **8**, 15140 (2017).
- [16] M. Girardi-Schappo, O. Kinouchi, and M. H. R. Tragtenberg, Critical avalanches and subsampling in map-based neural networks coupled with noisy synapses, *Phys. Rev. E* **88**, 024701 (2013).
- [17] T. T. Carvalho, A. J. Fontenele, M. Girardi-Schappo, T. Feliciano, L. A. Aguiar, T. P. Silva, N. A. De Vasconcelos, P. V. Carelli, and M. Copelli, Subsampled directed-percolation models explain scaling relations experimentally observed in the brain, *Front. Neural Circ.* **14**, 576727 (2021).
- [18] J. Touboul and A. Destexhe, Power-law statistics and universal scaling in the absence of criticality, *Phys. Rev. E* **95**, 012413 (2017).
- [19] N. Brunel, Dynamics of sparsely connected networks of excitatory and inhibitory spiking neurons, *J. Comput. Neurosci.* **8**, 183 (2000).
- [20] E. T. Jaynes, Information theory and statistical mechanics, *Phys. Rev.* **106**, 620 (1957).
- [21] G. Tkačik, T. Mora, O. Marre, D. Amodei, S. E. Palmer, M. J. Berry, and W. Bialek, Thermodynamics and signatures of criticality in a network of neurons, *Proc. Natl. Acad. Sci. USA* **112**, 11508 (2015).
- [22] J. Shlens, G. D. Field, J. L. Gauthier, M. I. Grivich, D. Petrusca, A. Sher, A. M. Litke, and E. Chichilnisky, The structure of multi-neuron firing patterns in primate retina, *J. Neurosci.* **26**, 8254 (2006).
- [23] A. Tang, D. Jackson, J. Hobbs, W. Chen, J. L. Smith, H. Patel, A. Prieto, D. Petrusca, M. I. Grivich, A. Sher *et al.*, A maximum entropy model applied to spatial and temporal correlations from cortical networks in vitro, *J. Neurosci.* **28**, 505 (2008).
- [24] C. Savin and G. Tkačik, Maximum entropy models as a tool for building precise neural controls, *Curr. Opin. Neurobiol.* **46**, 120 (2017).
- [25] C. I. Sampaio Filho, L. de Arcangelis, H. J. Herrmann, D. Plenz, P. Kells, T. L. Ribeiro, and J. S. Andrade, Jr., Ising-like model replicating time-averaged spiking behaviour of in vitro neuronal networks, *Sci. Rep.* **14**, 7002 (2024).

- [26] T. Mora, S. Deny, and O. Marre, Dynamical criticality in the collective activity of a population of retinal neurons, *Phys. Rev. Lett.* **114**, 078105 (2015).
- [27] N. Lotfi, A. J. Fontenele, T. Feliciano, L. A. A. Aguiar, N. A. P. de Vasconcelos, C. Soares-Cunha, B. Coimbra, A. J. Rodrigues, N. Sousa, M. Copelli, and P. V. Carelli, Signatures of brain criticality unveiled by maximum entropy analysis across cortical states, *Phys. Rev. E* **102**, 012408 (2020).
- [28] M. Girardi-Schappo, L. Brochini, A. A. Costa, T. T. Carvalho, and O. Kinouchi, Synaptic balance due to homeostatically self-organized quasicritical dynamics, *Phys. Rev. Res* **2**, 012042(R) (2020).
- [29] S. Sakata and K. D. Harris, Laminar structure of spontaneous and sensory-evoked population activity in auditory cortex, *Neuron* **64**, 404 (2009).
- [30] G. Paxinos and C. Watson, *The Rat Brain in Stereotaxic Coordinates: Hard Cover Edition* (Elsevier, Amsterdam, 2006).
- [31] J. H. Siegle, A. C. López, Y. A. Patel, K. Abramov, S. Ohayon, and J. Voigts, Open Ephys: an open-source, plugin-based platform for multichannel electrophysiology, *J. Neural Eng.* **14**, 045003 (2017).
- [32] C. Rossant, S. N. Kadir, D. F. Goodman, J. Schulman, M. L. Hunter, A. B. Saleem, A. Grosmark, M. Belluscio, G. H. Denfield, A. S. Ecker *et al.*, Spike sorting for large, dense electrode arrays, *Nat. Neurosci.* **19**, 634 (2016).
- [33] M. E. Newman and G. T. Barkema, *Monte Carlo Methods in Statistical Physics* (Clarendon, New York, 1999).
- [34] K. Pearson, Notes on the history of correlation, *Biometrika* **13**, 25 (1920).
- [35] T. Mora and W. Bialek, Are biological systems poised at criticality? *J. Stat. Phys.* **144**, 268 (2011).
- [36] N. Lotfi, T. Feliciano, L. A. A. Aguiar, T. P. L. Silva, T. T. A. Carvalho, O. A. Rosso, M. Copelli, F. S. Matias, and P. V. Carelli, Statistical complexity is maximized close to criticality in cortical dynamics, *Phys. Rev. E* **103**, 012415 (2021).